IOP Publishing Smart Materials and Structures
Smart Mater. Struct. 28 (2019) 025005 (11pp) https://doi.org/10.1088/1361-665X/aaeceb

Adaptive metamaterials for broadband sound absorption at low frequencies

Yunhong Liao[1], Xiaoming Zhou[1], Yangyang Chen[2] and Guoliang Huang[2]

[1] Key Laboratory of Dynamics and Control of Flight Vehicle, Ministry of Education and School of Aerospace Engineering, Beijing Institute of Technology, Beijing 100081, People's Republic of China
[2] Department of Mechanical and Aerospace Engineering, University of Missouri, Columbia, MO 65211, United States of America

E-mail: zhxming@bit.edu.cn

Received 30 July 2018, revised 29 October 2018
Accepted for publication 31 October 2018
Published 20 December 2018

Abstract

We propose and design a new adaptive sound absorption metamaterial targeting broadband airborne noise at extremely low frequencies. The metamaterial consists of two piezoelectric smart elements: a circular aluminum membrane with surface-bonded piezoelectric films controlled by shunting circuits enclosed with an air cavity for nearly total acoustic absorption at narrow-band frequencies; a hybrid-circuit shunted piezoelectric stack which is mechanically grounded attached to the center of the membrane for purely stiffness control to broaden this high-absorption bandwidth. A piezoelectric-structural-acoustic coupled model is firstly developed to evaluate the sound absorption of the metamaterial. We then perform analytical and numerical tests on metamaterials with and without the piezoelectric stack to design a metamaterial with broadband absorption at desired low frequencies. The underlying adaptive mechanism is to automatically regulate the effective acoustic resistance and reactance of the metamaterial to achieve impedance match conditions, according to different frequencies of inputs. Our numerical results demonstrate that the absorption coefficient of the adaptive metamaterial can be greater than 0.9 in the frequency region, 112–236 Hz with the relative bandwidth being around 0.7. The metamaterial thickness is 30 mm, which is nearly 1/65.6 wavelength of the central frequency of the absorption band. The proposed adaptive metamaterial may open a new avenue towards broadband sound absorption at extremely low frequencies.

Keywords: acoustic metamaterials, adaptive metamaterials, sound absorption

(Some figures may appear in colour only in the online journal)

1. Introduction

Airborne noises in our daily life produce a lot of trouble to both human's physical and mental health. To tackle this issue, various types of soundproof materials and/or structures for noise-control applications have been developed [1–6]. For example, foam materials [1] or micro-perforated plates [2, 3], which have been widely implemented in industrial applications, absorb sounds by viscous damping that happens in microscales. For linear responses, the frictional force is proportional to the particle oscillation rate; hence, the dissipative power will be extremely weak at low frequencies. To effectively dissipate low-frequency sounds, foam materials have to be very bulky as dictated by the causality principle [7]. Designing light-weight and compact materials for broadband low-frequency sound absorption is therefore highly desirable, which, however, presents strong challenges nowadays.

Acoustic metamaterials, which have been rapidly developed in the past decade, provided new efficient solutions in low-frequency mechanical energy dissipations with resonant microstructures. Recently, nearly total sound absorption metamaterials have been designed at narrow-band frequencies by covering a stretched membrane over an air cavity [8, 9]. The peak-absorption frequency can also be tuned to even lower by attaching small mass blocks on the membrane, such that the device is compact with the thickness far less than the operating wavelength. After that, several other absorptive metamaterial designs have been suggested. For example, normal quarter-wavelength acoustic damping tubes were bended and coiled into coplanar ones [10–12]. The improved absorber becomes highly compact with the thickness around one percent of the peak-absorption wavelength. By packing together subwavelength resonators of different operating frequencies, sound damping structures that could work over the relatively broad frequency band have been achieved [13–15]. The coherent perfect absorption, originally found in optics, has recently been verified in acoustics [16, 17]. To totally absorb sounds incident from one side, the control wave with the same amplitude but opposite phase is used, propagating inversely from the other side. It has also been found that absorption coefficients can take any values from unity to zero, depending on the relative phase between the incident and control waves. Currently available metamaterial absorbers, including those mentioned above, tend to share certain characteristics that they work in narrow bands centered at multiple resonant frequencies. In addition, they are passive systems implying that the sound absorption ability will be not tunable once absorber samples are fabricated.

Tunable sound absorption using active materials and structures has been studied for a long time [18–27]. The active sound cancelation technique is the method for eliminating unwanted sounds by an additional feedforward control power source [18]. Active noise canceling technique is best suited for acoustic cavity and duct based systems, and for the periodic sounds than random ones. On the other hand, piezoelectric materials, which are compact, lightweight, and can be easily tuned by shunting circuits, have been extensively implemented for the damper design in structures, causing an essential change of dissipation capabilities. This technique has also been actively applied in lots of sound control applications. Passive sound absorbers combined with piezoelectric membranes can achieve the sound absorption at a single frequency controlled by a feedback loop [19]. Thin micro-perforated plates attached with piezoelectric patches and electrical circuits were suggested, where the sound absorption can be improved by tuning shunting circuits [20]. When the micro-perforated panel was made by flexible Polyvinylidene fluoride piezoelectric film, sound absorption could be also improved by using the shunt-damping technology [21]. Hybrid multilayered cells consisting of porous damping material and piezoelectric plate were investigated, in which active control has been proved to enhance sound transmission loss and absorption [22, 23]. Acoustic absorbing systems designed with active materials have shown great potentials in the damping enhancement. However, the tunable and broadband manipulation on sound absorption at extremely low frequencies has not been fully solved.

Recently, authors have proposed a different mechanism for broadband noise control based on adaptive metamaterials that involve piezoelectric materials with shunting circuits. When both negative capacitance and inductance are introduced into the circuit, the extremely wideband flexural wave bandgap has been created [28]. In the later study, we extended this concept to the acoustic-structural interaction system, and demonstrated that high sound transmission loss can be achieved in broadband frequency and angular spectrum [29]. In this work, we further apply the adaptive-metamaterial concept for the design of small-size active cells with broadband sound absorption at extremely low frequencies. In section 2, we first illustrate the design of the adaptive metamaterial. An analytical model considering the piezoelectric-structure-acoustic coupling is then developed for the theoretical estimation of the sound absorption. In section 3, numerical examples and discussions are provided, from which broadband sound absorptions at low frequencies are verified and physical mechanisms are explained. A brief summary is finally provided in section 4.

2. Analytical model of the adaptive metamaterial

2.1. Design of the adaptive metamaterial

Figure 1 shows the schematic of the proposed adaptive metamaterial. The initial structure of the metamaterial consists of a circular aluminum membrane, enclosed with an air cavity of the 30 mm depth. The Young's modulus, Poisson's ratio and mass density for this aluminum membrane are selected as 70 GPa, 0.34, and 2730 kg m^{-3}, respectively. This initial construction possesses the hybrid resonance of acoustic-membrane interactions, which could produce complete sound absorptions at multiple isolated frequencies. The major advantage of the absorptive structure is the deep-subwavelength size with the thickness less than the operating wavelength by up to two orders of magnitude [8, 9]. In the current design, the active strategy, which has been widely implemented previously [19–23], is employed to render tunable peak absorption frequencies as an attempt to extend the bandwidth of the total acoustic absorption. To this end, two piezoelectric films (PZT-5H) of thickness 0.2 mm with the shunting circuits are bonded on both sides of the aluminum membrane. Acoustic resistance and reactance of the system then become relevant to the shunting circuit, which will play a critical role to regulate the sound absorption performance. Furthermore, the membrane's mobility is constrained by the hybrid circuit shunted piezoelectric stack (PMN-0.33PT), one end of which is attached to the center of the membrane, while the other side is attached to a rigid cylinder fixed to the ground, which represents the fixed boundary condition. The piezoelectric stack with shunting circuits that involve negative capacitance and negative inductance could behave like an elastic spring with the frequency dependent stiffness [28, 29]. In our previous sound-reflection design [29], the circuit parameters of the piezoelectric stack have been optimized so that the frequency dependent stiffness of the stack follows the high transmission-loss trajectory, giving rise to the giant sound reflection in both broad frequency and angular bands. In this work, the piezoelectric stack with shunting circuits is expected to function in the similar manner as tracing the peak-absorption trajectory for the broadband sound absorption.

It is important to develop a piezoelectric-structural-acoustic coupled model, which is necessary to discover the

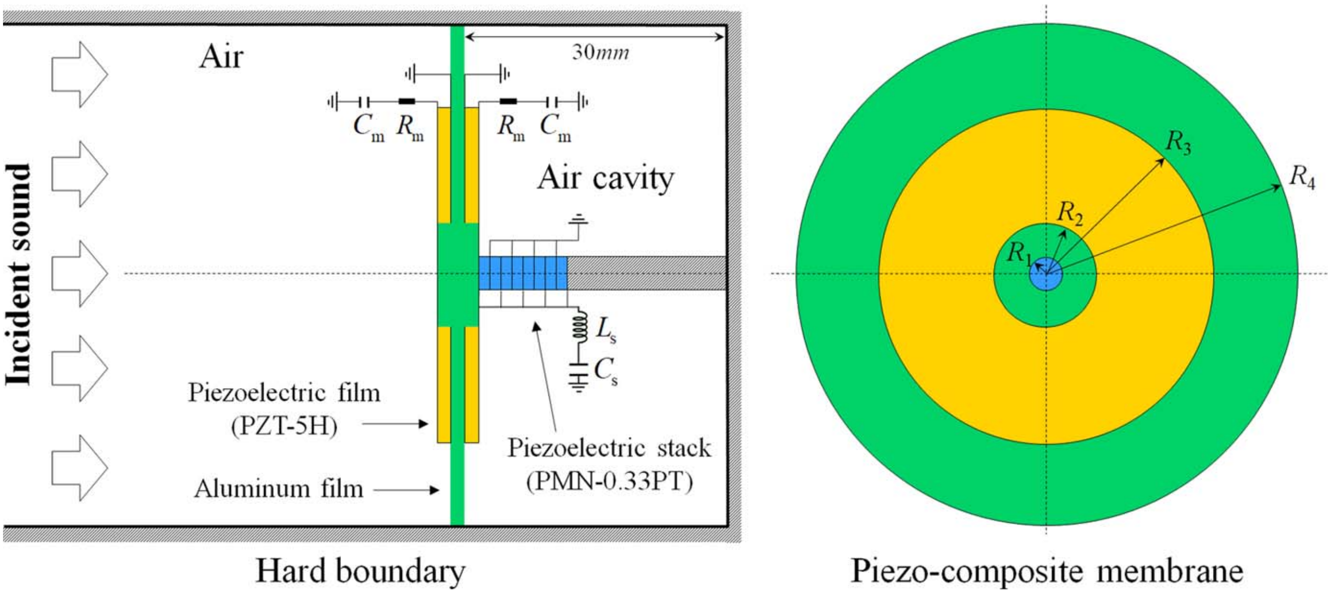

Figure 1. The schematic of adaptive metamaterials designed for broadband sound absorption at low frequencies.

working mechanism of broadband sound absorption. Some simplifications have to be made in order to formulate theoretically the total acoustic impedance as well as acoustic absorption of the adaptive metamaterials. We divide the compound membrane into four circular regions with different inner and outer radii $R_4/3 = R_3/2 = R_2 = 20R_1 = 20$ mm, as shown in figure 1. The innermost part ($r \leqslant R_1$) is the aluminum membrane of thickness 0.6 mm, which is constrained by the piezoelectric stack with a frequency dependent stiffness. The adjacent part ($R_1 \leqslant r \leqslant R_2$) is the aluminum membrane of the same thickness without the attached stack. The third region ($R_2 \leqslant r \leqslant R_3$) is the aluminum membrane of thickness 0.2 mm, which is covered on both sides with the piezoelectric film, and the remaining part ($R_3 \leqslant r \leqslant R_4$) is the membrane uncovered by the piezoelectric film. Each region of the composite membrane is modeled as the homogeneous plate following the Kirchhoff plate equation. Note that effective material parameters of sandwiched aluminum and piezoelectric membranes in the third region, which is requested by the analytical model, will be provided in section 2.3. The Kirchhoff plate equation for the jth region ($j = 1, 2, 3, 4$) of the membrane that undergoes only the transverse displacement $w_j(r)$ is given by [30, 31]

$$\nabla^4 w_j(r) - k_j^4 w_j(r) = \Delta P_j / B_j, \tag{1}$$

where $k_j^4 = \omega^2 \rho_j h_j / B_j$ and $B_j = \frac{E_j h_j^3}{12(1-\upsilon_j^2)}$ is the bending stiffness. The Young's modulus, Poisson's ratio, mass density, and thickness of the jth membrane region are represented respectively by E_j, υ_j, ρ_j, and h_j. ΔP_j that appears on the right-hand side of equation (1) refers to acoustic load. Based on above simplification, we will establish an analytical model to formulate the total acoustic impedance of the composite structure, which has an explicit relation to sound absorption of the system.

2.2. Sound absorption of adaptive metamaterials

Consider a plane acoustic wave that is normally incident on the adaptive metamaterial. Assume the low-frequency scenario, where the air wavelength is much greater than the membrane diameter, so that one can only consider the lowest order flexural mode of the membrane. In addition, assume that acoustic pressure loads are same in all membrane regions, i.e. $\Delta P_j = \Delta P$. Accordingly, the general solution to the flexural-wave equation $\nabla^4 w(r) - k^4 w(r) = \Delta P/B$ can be written in the following form [30]

$$w(r) = a_1 J_0(kr) + a_2 Y_0(kr) + a_3 I_0(kr) + a_4 K_0(kr) - \frac{\Delta P}{k^4 B}, \tag{2}$$

where $J_0(kr)$, $Y_0(kr)$, $I_0(kr)$, and $K_0(kr)$ are respectively the first and second kinds of the zeroth-order Bessel function, as well as the first and second kinds of zeroth-order modified Bessel function. Based on equation (2), the transverse displacement in the jth region ($j = 2, 3, 4$) can be expressed as

$$w_j(r) = a_1^{(j)} J_0(k_j r) + a_2^{(j)} Y_0(k_j r) + a_3^{(j)} I_0(k_j r) + a_4^{(j)} K_0(k_j r) - \frac{\Delta P}{k_j^4 B_j}, \tag{3}$$

where $a_1^{(j)}$, $a_2^{(j)}$, $a_3^{(j)}$, and $a_4^{(j)}$ are unknown coefficients to be determined from the continuity and boundary conditions.

Particular attention is given to the innermost region ($r \leqslant R_1$), which is constrained by the piezoelectric stack that functions pertinently as the spring of the stiffness K_s. Note that effective spring coefficient K_s of the stack is obtained as [28, 29]

$$K_s = \frac{E_p^{\mathrm{eff}} \pi R_1^2}{h_s}, \tag{4}$$

where h_s is the height of the stack, and E_p^{eff} is effective dynamic stiffness of the piezoelectric stack, given by [28, 32]

$$E_{\mathrm{p}}^{\mathrm{eff}} = \frac{E_{\mathrm{p}}^{E}}{1 - \frac{k_{33}^{2}}{1 + 1/(i\omega C_{\mathrm{p}}^{s} Z_{\mathrm{s}})}}, \tag{5}$$

where $k_{33} = \frac{d_{33}}{\sqrt{\varepsilon_{33}^{T} s_{33}^{E}}}$, $E_{\mathrm{p}}^{E} = \frac{1}{s_{33}^{E}}$, $C_{\mathrm{p}}^{s} = \frac{N_{\mathrm{s}}^{2} \pi R_{1}^{2} \varepsilon_{33}^{T}}{h_{\mathrm{s}}}$ and $Z_{\mathrm{s}} = \frac{1}{i\omega C_{\mathrm{s}}} + i\omega L_{\mathrm{s}}$ represent respectively the electromechanical coupling coefficient, the short-circuit Young's modulus, the capacitance of the piezoelectric stack and the circuit impedance. For more details, d_{33}, s_{33}^{E}, ε_{33}^{T} are the piezoelectric constant, short-circuit elastic compliance and dielectric coefficient at constant stress respectively. N_{s} is the number of the piezoelectric plate that constitutes the stack. L_{s} and C_{s} are the inductance and capacitance that are connected in series. Finally, the displacement equation of the innermost region need be modified by adding the spring force $-\overline{K} w_1$ to the source term of the flexural-wave equation as

$$B_1 \nabla^4 w_1(r) - \rho_1 h_1 \omega^2 w_1(r) = \Delta P - \overline{K} w_1(r), \tag{6}$$

where $\overline{K} = K_{\mathrm{s}}/\pi R_1^2$. Casting above equation into the standard form similar to equation (1), we have the new expression for the wavenumber $k_1^4 = (\rho_1 h_1 \omega^2 - \overline{K})/B_1$. According to equation (2), the displacement solution in the region of $r \leqslant R_1$ is expressed as

$$w_1(r) = a_1^{(1)} J_0(k_1 r) + a_3^{(1)} I_0(k_1 r) - \frac{\Delta P}{k_1^4 B_1} \tag{7}$$

herein the terms involving $Y_0(k_1 r)$ and $K_0(k_1 r)$ has been removed to ensure the finite solution at $r = 0$.

At the interface $r = R_j$ ($j = 1,\ 2,\ 3$), the continuity conditions of the displacement, the slope, the radial bending moment, and the shear force, are listed respectively as

$$w_j(R_j) = w_{j+1}(R_j) \tag{8}$$

$$\frac{dw_j(R_j)}{dr} = \frac{dw_{j+1}(R_j)}{dr} \tag{9}$$

$$B_j\left[\frac{d^2 w_j(R_j)}{dr^2} + \frac{\upsilon_j}{r}\frac{dw_j(R_j)}{dr}\right] = B_{j+1}\left[\frac{d^2 w_{j+1}(R_j)}{dr^2} + \frac{\upsilon_{j+1}}{r}\frac{dw_{j+1}(R_j)}{dr}\right] \tag{10}$$

$$B_j \frac{d}{dr}\left[\frac{d^2 w_j(R_j)}{dr^2} + \frac{1}{r}\frac{dw_j(R_j)}{dr}\right] = B_{j+1}\frac{d}{dr}\left[\frac{d^2 w_{j+1}(R_j)}{dr^2} + \frac{1}{r}\frac{dw_{j+1}(R_j)}{dr}\right]. \tag{11}$$

The displacement and its slope are zero at the outermost boundary $r = R_4$, leading to

$$w_4(R_4) = 0 \tag{12}$$

$$\frac{dw_4(R_4)}{dr} = 0. \tag{13}$$

By substituting displacement expressions (7) and (3) into the interface conditions (8)–(13), we can express all unknown coefficients $a_m^{(n)}$ in terms of acoustic load ΔP. Acoustic impedance of the composite membrane can then be obtained

$$Z_{\mathrm{mem}} = \frac{\Delta P}{i\omega \overline{w}}, \tag{14}$$

where $\overline{w}$ is the average displacement of the membrane, which is computed by integrating the displacement w_j over the corresponding region

$$\overline{w} = \sum_{j=1}^{4} \int\!\!\int_{S_j} w_j ds/(\pi R_4^2). \tag{15}$$

Acoustic impedance of the air cavity is known as [33]

$$Z_{\mathrm{air}} = -i\rho_0 c_0 \cot(k_0 h_{\mathrm{c}}), \tag{16}$$

where $\rho_0 = 1.29\ \mathrm{kg\ m^{-3}}$ and $c_0 = 343\ \mathrm{m\ s^{-1}}$ are the density and sound velocity of the air, k_0 is the wave number and h_{c} is the cavity depth. The total acoustic impedance of adaptive metamaterial is the summation of acoustic impedances of the membrane and cavity, written in the normalized form with respect to the air as

$$Z_{\mathrm{t}} = \frac{Z_{\mathrm{mem}} + Z_{\mathrm{air}}}{\rho_0 c_0} = R_{\mathrm{t}} + X_{\mathrm{t}} i, \tag{17}$$

where R_{t} and X_{t}, which are the real and imaginary parts of Z_{t}, represent the normalized acoustic resistance and reactance of the system. Finally, acoustic absorption coefficient α of the adaptive metamaterial can be calculated from

$$\alpha = \frac{4R_{\mathrm{t}}}{(1 + R_{\mathrm{t}})^2 + X_{\mathrm{t}}^2}. \tag{18}$$

2.3. Effective material parameters of sandwiched aluminum and piezoelectric membranes

We first evaluate the effective elastic constant of the piezoelectric film with the shunting circuit. Assume the plane-stress state for the thin piezoelectric film, which is placed on the x_1–x_2 plane. The constitutive equation of the piezoelectric film is written as [34]

$$\begin{bmatrix} \gamma_{11} \\ \gamma_{22} \\ D_3 \end{bmatrix} = \begin{bmatrix} s_{11}^{E} & s_{12}^{E} & d_{31} \\ s_{12}^{E} & s_{11}^{E} & d_{31} \\ d_{31} & d_{31} & \varepsilon_{33}^{T} \end{bmatrix} \begin{bmatrix} \sigma_{11} \\ \sigma_{22} \\ E_3 \end{bmatrix}, \tag{19}$$

where γ_{11}, γ_{22} are normal strains, σ_{11}, σ_{22} are normal stresses, and s_{11}^{E}, s_{12}^{E} denote the short-circuit elastic compliance. D_3 and E_3 are the out-of-plane electric displacement and electric field. ε_{33}^{T} and d_{31} are the dielectric constant and piezoelectric coefficient. Introduce the shunting circuit, in which the capacitance C_{m} and resistance R_{m} are connected in series. The impedance of the circuit reads $Z_{\mathrm{m}} = R_{\mathrm{m}} + \frac{1}{i\omega C_{\mathrm{m}}}$, which satisfies the following electric current equation [35]

$$E_3 h_{\mathrm{m}}/Z_{\mathrm{m}} = -i\omega S_{\mathrm{m}} D_3, \tag{20}$$

where h_{m} and S_{m} ($=\pi R_3^2 - \pi R_2^2$) are the thickness and surface area of the piezoelectric film. Substitution of (20) into the third equation of (19) leads to the electric field E_3 that is written in terms of σ_{11} and σ_{22}. Using this expression to eliminate E_3 in the first two equations of (19), we get [34]

$$\begin{bmatrix}\gamma_{11}\\ \gamma_{22}\end{bmatrix} = \begin{bmatrix} s_{11}^E - \dfrac{i\omega Z_m d_{31}^2 S_m h_m^{-1}}{1+i\omega Z_m C_p^m} & s_{12}^E - \dfrac{i\omega Z_m d_{31}^2 S_m h_m^{-1}}{1+i\omega Z_m C_p^m} \\ s_{12}^E - \dfrac{i\omega Z_m d_{31}^2 S_m h_m^{-1}}{1+i\omega Z_m C_p^m} & s_{11}^E - \dfrac{i\omega Z_m d_{31}^2 S_m h_m^{-1}}{1+i\omega Z_m C_p^m} \end{bmatrix} \begin{bmatrix}\sigma_{11}\\ \sigma_{22}\end{bmatrix}, \tag{21}$$

where C_p^m is the capacitance of the piezoelectric film, given by

$$C_p^m = \varepsilon_{33}^T S_m / h_m. \tag{22}$$

It is known that the constitutive relation that governs the plane-stress elasticity is given by

$$\begin{bmatrix}\gamma_{11}\\ \gamma_{22}\end{bmatrix} = \begin{bmatrix} \dfrac{1}{E_m} & -\dfrac{\upsilon_m}{E_m} \\ -\dfrac{\upsilon_m}{E_m} & \dfrac{1}{E_m} \end{bmatrix} \begin{bmatrix}\sigma_{11}\\ \sigma_{22}\end{bmatrix}. \tag{23}$$

By matching equations (21) and (23), we can retrieve the Young's modulus and Poisson ratio of the piezoelectric film as follows

$$E_m = \frac{h_m(1+i\omega Z_m C_p^m)}{h_m s_{11}^E(1+i\omega Z_m C_p^m) - i\omega Z_m d_{31}^2 S_m} \tag{24}$$

$$\upsilon_m = -\frac{s_{12}^E(1+i\omega Z_m C_p^m) - i\omega Z_m d_{31}^2 S_m h_m^{-1}}{s_{11}^E(1+i\omega Z_m C_p^m) - i\omega Z_m d_{31}^2 S_m h_m^{-1}}. \tag{25}$$

According to the homogenization method, the average density of sandwiched aluminum and piezoelectric membranes follows

$$\rho_{eff} = \frac{h_a\rho_a + 2h_m\rho_m}{h_a + 2h_m}, \tag{26}$$

where $h_a = 0.2$ mm is the thickness of aluminum membrane of the region $R_2 \leqslant r \leqslant R_3$. ρ_a and ρ_m are the densities of the aluminum and piezoelectric film. The overall bending stiffness of the sandwiched membrane is given by [36]

$$B_{eff} = \frac{E_m[(2h_m + h_a)^3 - h_a^3]}{12(1-\upsilon_m^2)} + \frac{E_a h_a^3}{12(1-\upsilon_a^2)}, \tag{27}$$

where E_a and υ_a denote the Young's modulus and Poisson's ratio of the aluminum membrane.

The analytical model developed in this section will be used to design the metamaterial parameters and demonstrate the superior sound absorption. Note that the developed model, based on the theory of plate dynamics and piezoelectricity, serves specifically to our design, where equations are built and solved with real geometric and circuit parameters, aiming to provide a deep insight into the piezoelectric-structural-acoustic coupling. The model has related all microstructural parameters to the total acoustic impedance. Analytical solutions between circuit parameters and acoustic impedance will be presented in the following section.

Table 1. Material parameters of piezoelectric stack and film.

Piezoelectric stack (PMN-33%PT) [28]			
c_{11}^E	115.0 Gpa	e_{15}	10.1 C m^{-2}
c_{12}^E	103.0 Gpa	e_{31}	−3.9 C m^{-2}
c_{13}^E	102.0 Gpa	e_{33}	20.3 C m^{-2}
c_{33}^E	103.0 Gpa	d_{33}	2820.0 × 10^{-12} C N^{-1}
c_{44}^E	69.0 Gpa	ε_{11}^S	1434.0ε_0
c_{66}^E	66.0 Gpa	ε_{33}^S	680.0ε_0
s_{33}^E	119.6 × 10^{-12}m^{2}N^{-1}	ε_{33}^T	8200.0ε_0
Piezoelectric film (PZT-5H) [34]			
s_{11}^E	16.5 × 10^{-12} m^2 N^{-1}	s_{12}^E	−4.78 × 10^{-12} m^2 N^{-1}
d_{31}	−2.74 × 10^{-10} C N^{-1}	ε_{33}^T	3.01 × 10^{-8} F m^{-1}
ρ_m	7500 kg m^{-3}		

3. Results and discussions

In this section, we characterize the sound absorption performance of adaptive metamaterials with different sets of circuit parameters. The shunting circuits are used in both piezoelectric membrane and piezoelectric stack, while their functions for monitoring sound absorption are different. Therefore, these will be examined in two separate systems, structured membranes with and without the piezoelectric stack. Material parameters of piezoelectric materials used in our model have been listed in table 1.

Let us first study the sound absorption of structured membranes without the piezoelectric stack. To dissipate the acoustic energy, it is necessary to introduce the resistor R_m into the shunting circuit of piezoelectric membranes. Figure 2(a) plots the absorption spectrum calculated by the analytical model in the case that the resistor with $R_m = 180\ \Omega$ is only considered in the circuit. The result displays the maximum absorption coefficient 0.3 near the frequency 250 Hz. When a positive capacitance with $C_m = 350$ nF is added to the circuit, the absorption behavior becomes even worse, where the maximum damping coefficient decrease to less than 0.1. However, it is found that the nearly total absorption can be achieved by introducing the negative capacitance of $C_m = -350$ nF, as evidenced in figure 2(a). Note that finite element simulations of the practical structure are also conducted based on a commercial software package comsol Multiphysics, as plotted by the circles in figure 2(a). The figure inset shows the pressure field and displacement profile of the structure at 256 Hz. The results support the assumptions made in the analytic model, which state that the membrane indeed undergoes the lowest order flexural motion, and acoustic pressures are uniformly distributed in the radial

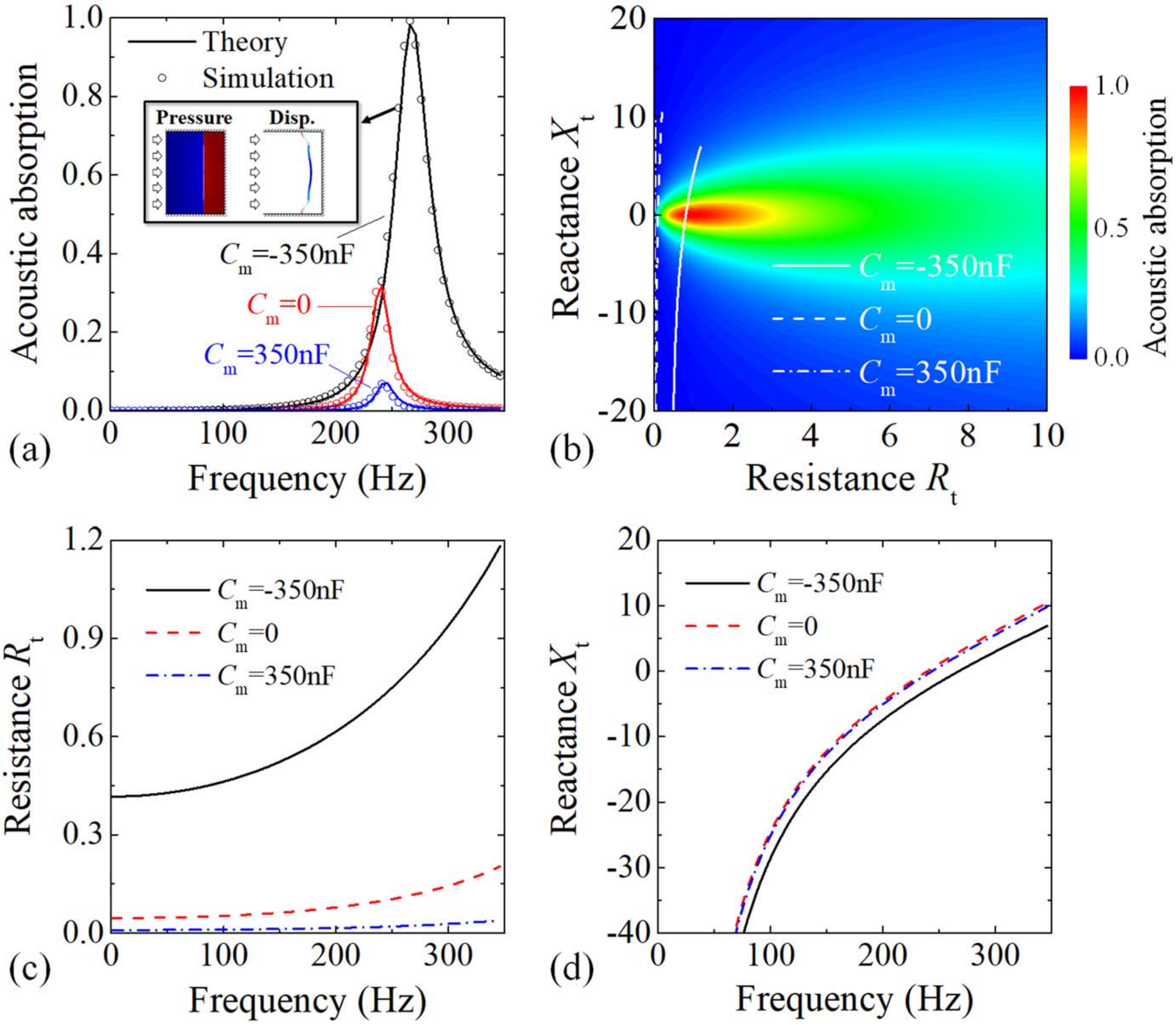

Figure 2. (a) Sound absorption spectrum of adaptive metamaterials without the piezoelectric stack in three cases of circuit parameters of the piezoelectric film: $R_m = 180\ \Omega$, and $C_m = -350$ nF, 0, or 350 nF; (b) contour plot of absorption coefficient α calculated from equation (18) against different acoustic resistance R_t and reactance X_t, in which the $R_t - X_t$ trajectories in three cases are shown; Acoustic resistance (c) and reactance (d) of the system against the frequency in case of three circuit parameters.

direction. Excellent agreements between numerical and theoretical results in three cases also validate the accuracy of the analytical model.

The physical mechanism of the sound absorption enhancement with the negative capacitance can be understood from the absorption-impedance formulas of equation (18). Figure 2(b) shows the contour plot of absorption coefficient α calculated based on equation (18) with different prescribed acoustic resistance R_t and reactance X_t. It is observed that the high acoustic absorption occurs in the region near the parameter set $R_t = 1$, $X_t = 0$, which describes the perfect impedance match to the airborne sound. Therefore, the circuit parameters should be modulated so that the resultant resistance–reactance trajectory of the absorptive metamaterial passes through that region. When $C_m \geqslant 0$, R_t is much less than one as shown in figure 2(c), resulting in that the $R_t - X_t$ path is far from the high-absorption zone (figure 2(b)). When the negative capacitance is considered, R_t can be significantly enhanced, approaching the desired value $R_t = 1$ at a specific frequency (figure 2(c)). Besides, the negative capacitance shows the weak influence on the acoustic reactance compared between the three cases, as illustrated in figure 2(d). As a result, the corresponding $R_t - X_t$ trajectory could go across the high-absorption zone, explaining the nearly total absorption in case of the negative capacitance $C_m = -350$ nF. For further verification, the frequency response of acoustic resistance and reactance in a wide range of capacitance values $-400\ \text{nF} \leqslant C_m \leqslant 400\ \text{nF}$ are computed as shown in figures 3(a) and (b) respectively. Results confirm that the negative capacitance, which induces the significant enhancement of acoustic resistance, is necessary for the nearly perfect absorption in the narrow frequency band.

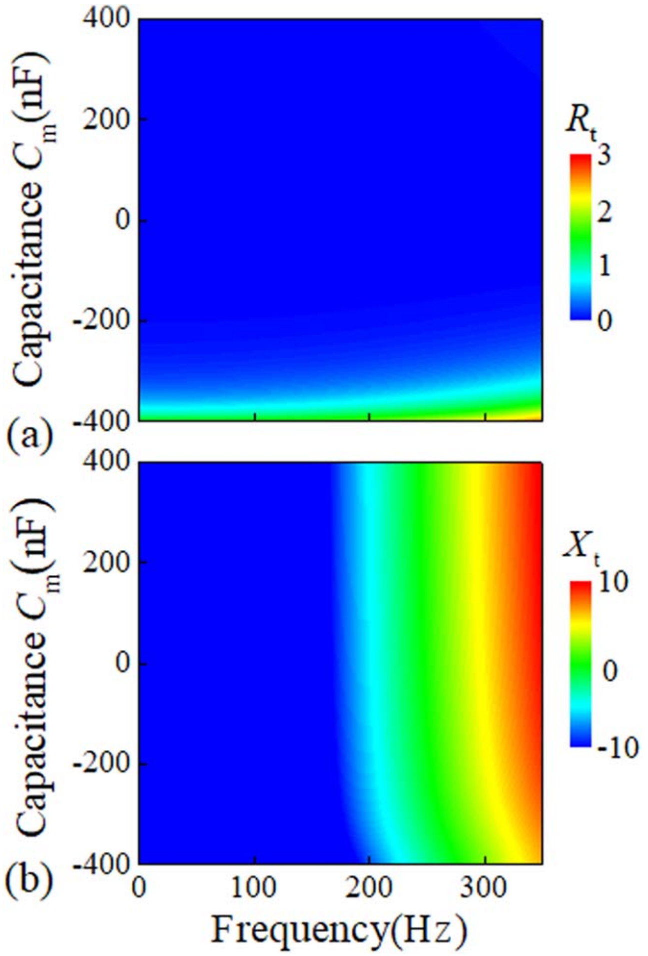

Figure 3. Analytic results of acoustic resistance R_t and reactance X_t in a wide range of capacitance values -400 nF $\leqslant C_m \leqslant 400$ nF of adaptive metamaterials without the piezoelectric stack.

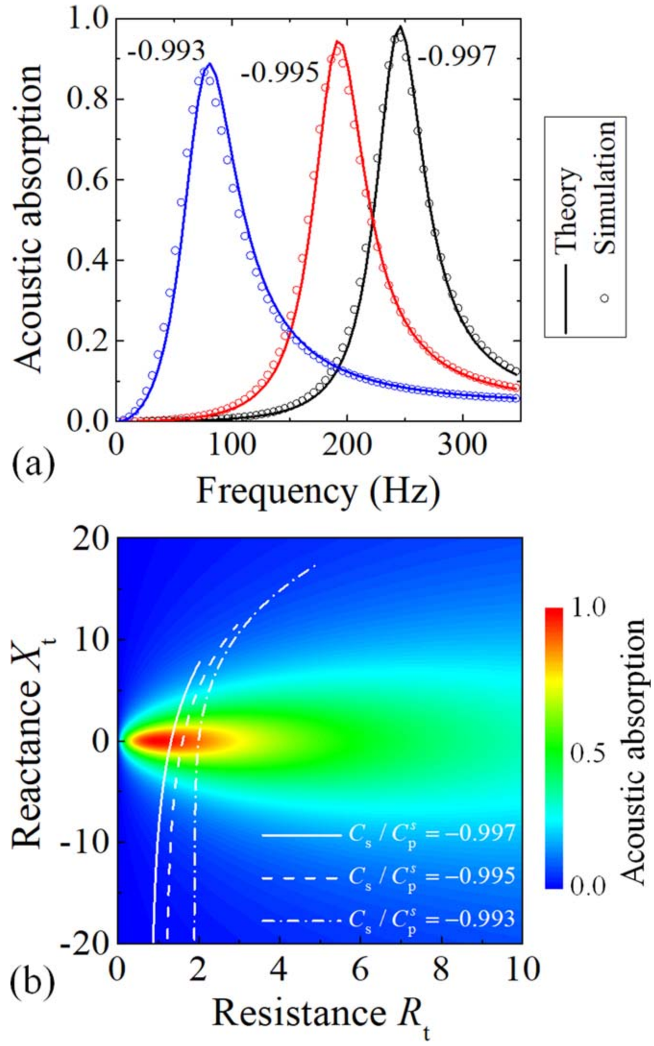

Figure 4. (a) Sound absorption spectrum of adaptive metamaterials with the piezoelectric stack, in which three capacitance values $C_s/C_p^s = -0.993$, -0.995, and -0.997 are considered in the shunting circuit of the stack; (b) the corresponding $R_t - X_t$ trajectories in the contour plot of absorption coefficient against R_t and X_t.

Now we evaluate the sound absorption capability of structured metamaterials with the piezoelectric stack. Notice that geometric parameters of the stack are chosen as $N_s = 8$ and $h_s = 10$ mm. If there is only the capacitance C_s in the shunting circuit of the piezoelectric stack, effective stiffness of the stack is irrelevant to the frequency. It can vary upon the change of C_s, becoming negative in the range of capacitance values $-1 \leqslant C_s/C_p^s \leqslant k_{33}^2 - 1$. Acoustic absorption spectrum in case of three capacitance values $C_s/C_p^s = -0.993$, -0.995, and -0.997 is shown in figure 4(a), where circuit parameters for the piezoelectric membrane are chosen as $R_m = 55\,\Omega$ and $C_m = -400$ nF. Note that effective stiffness will approach a larger negative value for a smaller $|C_s|$ in above three cases. Due to the negative-stiffness effect of the piezoelectric stack, the overall stiffness of the composite membrane will be reduced, accounting for the downward shifting of peak absorption frequency. The $R_t - X_t$ trajectories corresponding to three cases are plotted in figure 4(b). They all pass across the high-absorption zone centered at $R_t = 1$, $X_t = 0$. Analytic predictions have the good agreement with simulation results. It is therefore concluded that the negative capacitance adhered to the stack plays the role of lowering the peak absorption frequency, meanwhile the nearly total acoustic absorption can be maintained.

Consider further that negative capacitance and inductance are both connected to the piezoelectric stack. In this case, the stack with shunting circuits behaves like an elastic spring whose effective stiffness varies with the frequency, as governed by equation (5). In previous studies, the dispersive stiffness of the stack has been used to trace adaptively the high transmission-loss trajectory for the broadband sound insulation [29]. In the present study, the stack is expected to serve the broadband sound absorption. To this end, we calculate acoustic absorption for different stiffness coefficients as shown in figure 5(a), in which $R_m = 55\,\Omega$ and $C_m = -400$ nF are used. The high-absorption trajectory is clearly seen with the frequency proportional to the stiffness. It is important to note that this desired high-absorption curve matches very well with the frequency dependent stiffness of piezoelectric stacks. Figure 5(a) shows by the dashed line the

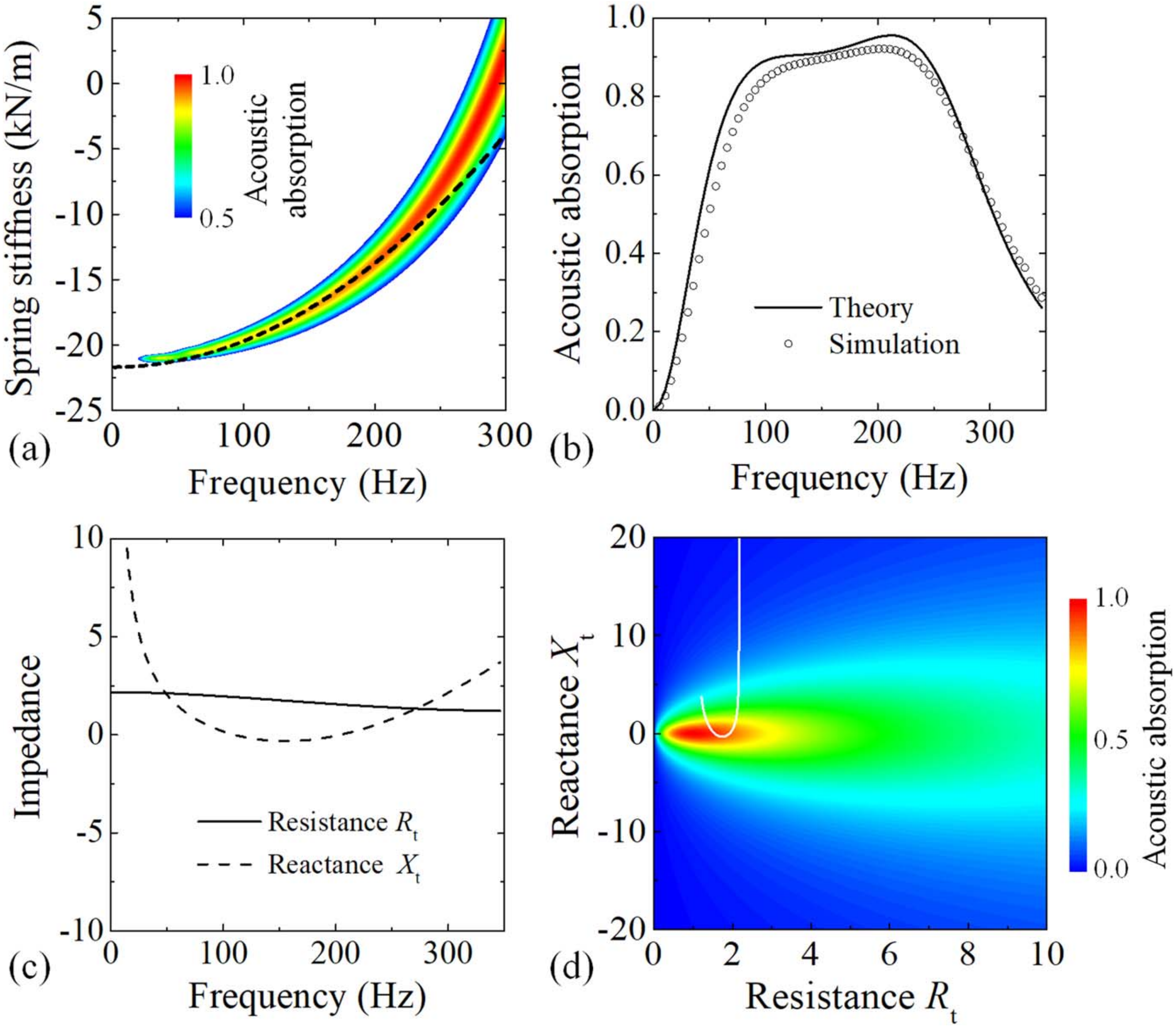

Figure 5. (a) Sound absorption spectrum for different stiffness coefficients of the spring that is mimicked by the piezoelectric stack, in which the dashed line refers to the frequency dependent effective stiffness that can be practically realized by the stack; (b) Sound absorption spectrum of adaptive metamaterials, whose circuit parameters have been optimized to trace adaptively the high absorption trajectory; (c) Acoustic resistance and reactance of adaptive metamaterials against the frequency; (d) the corresponding $R_t - X_t$ trajectory in the contour plot of absorption coefficient against R_t and X_t. Circuit parameters $R_m = 55\ \Omega$, $C_m = -400$ nF, $C_s = -0.9925C_p^s$, and $L_s = -1.2$H are used.

dispersive stiffness of the stack with optimized circuit parameters $C_s/C_p^s = -0.9925$ and $L_s = -1.2$H. The result in figure 5(b) reveals that the high-absorption bandwidth can be indeed widened due to the adaptive stiffness of piezoelectric stack. Theoretical predictions have good match to simulation results of the actual structure; the latter shows the absorption coefficient over 0.8 in the frequency range 86–256 Hz with the relative bandwidth 1.0. The broadened absorption bandwidth can be also understood by the impedance result of adaptive metamaterials (figure 5(c)). It is seen in figure 5(d) that the $R_t - X_t$ trajectory forms the J-shaped profile, so that more numbers of frequency points are distributed in the high absorption region. In another example, we have optimized a different set of circuit parameters $R_m = 180\ \Omega$, $C_m = -350$ nF, $C_s/C_p^s = -0.9935$, and $L_s = -1.4$H for pursuing higher absorption coefficients, but with a small decreasing of the absorption bandwidth. Corresponding results are provided in figure 6 with the similar fashion to figure 5. The absorption coefficient of simulation results has reached 0.9 in the frequency range 112–236 Hz with the relative bandwidth 0.7. Note that the thickness of the adaptive meta-composite is 30 mm, which is nearly $1/65.6$ wavelength of the band's center frequency 174 Hz.

The presented results have clearly disclosed the working mechanism of the piezoelectric film and stack in achieving the broadband and low-frequency sound absorption. It can be found that the sound absorption frequency range can be flexibly tuned by the electric parameters of circuits shunted to piezoelectric elements, allowing for the optimization of the desired absorption behavior for any reasonable structural

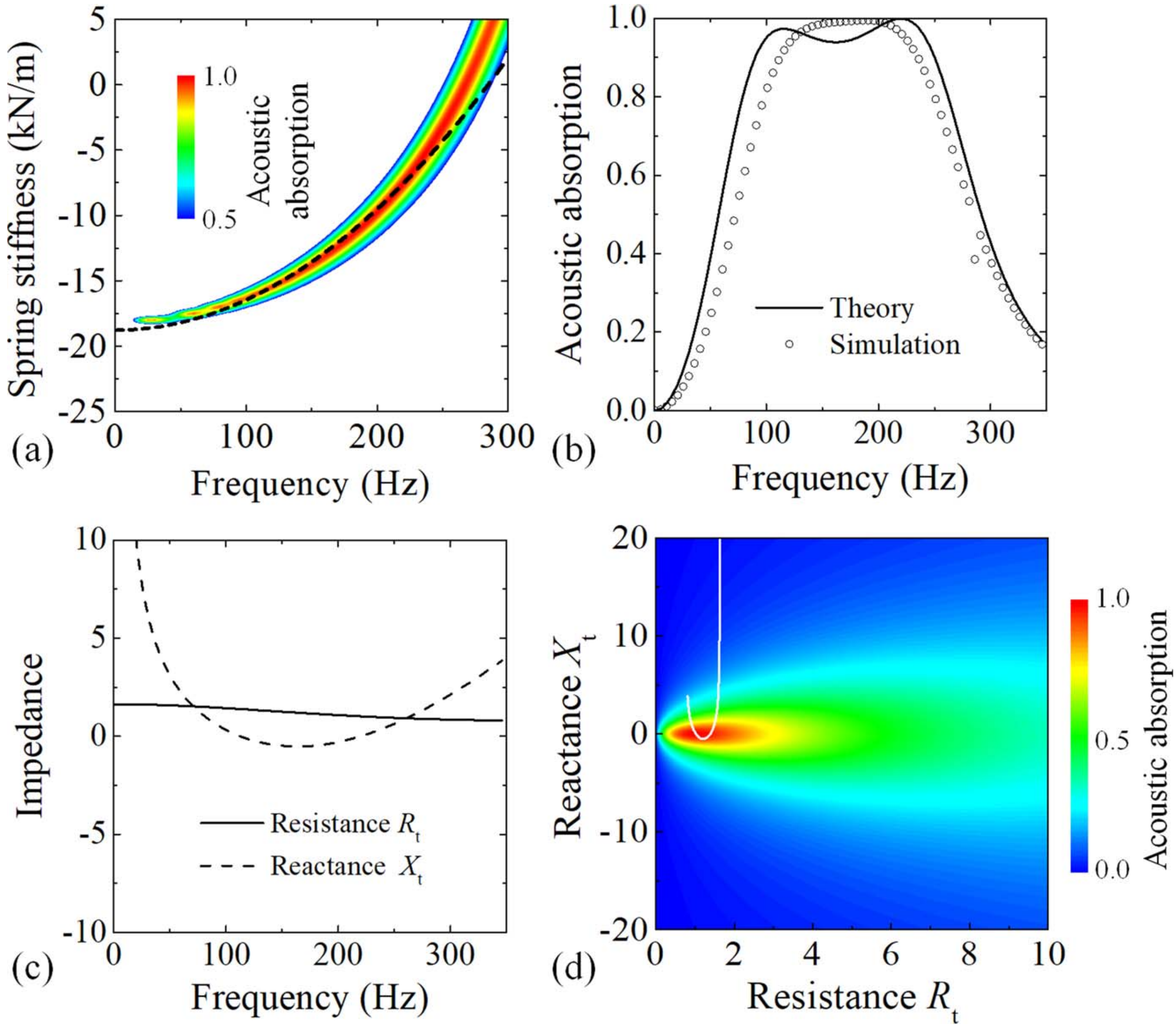

Figure 6. Results similar to figure 5 for adaptive metamaterials with circuit parameters $R_m = 180\ \Omega$, $C_m = -350$ nF, $C_s = -0.9935C_p^s$, and $L_s = -1.4$H.

parameters, including membrane material and size parameters. The developed analytical model serves as an efficient tool for rapidly optimizing circuit parameters according to the high-absorption condition $R_t = 1$, $X_t = 0$. Therefore, the design optimization of broadband absorptive metamaterials targeting practical applications can be anticipated in further study.

4. Conclusion

In our previous studies, we have proposed a new class of adaptive metamaterials that contain the piezoelectric stack with shunting circuits. The piezoelectric stack with both negative capacitance and inductance behaves like an elastic spring with effective stiffness that could change proportional to the excitation frequency. This adaptive stiffness effect can be employed to attain super broadband structure-borne bandgaps [28], as well as broadband sound insulation in both frequency and angular spectrum [29]. The main contribution of this study is to demonstrate the application of the adaptive stiffness effect of piezoelectric stack on the design of broadband sound absorbing structure.

The base construction of the proposed absorptive meta-composite consists of a circular aluminum membrane enclosed with an air cavity. Two Piezoelectric films (PZT-5H) are bonded on both sides of the aluminum membrane. The hybrid shunted piezoelectric stack (PMN-0.33PT) supports the membrane's center with the other end fixed to the ground. An analytical piezoelectric-structural-acoustic coupled model has been developed for the evaluation of sound absorption of the meta-composite. It is found from the analytical model that high acoustic absorption occurs in the region near the impedance match point $R_t = 1$, $X_t = 0$ with respect to the background air. When the electric circuit of piezoelectric film involves only the resistor, the $R_t - X_t$ trajectory stays far from the matching point, leading to the weak sound absorption. The negative capacitance, which induces the significant enhancement of acoustic resistance R_t, is necessary for the nearly total absorption in the narrow frequency band. To enlarge the high absorption bandwidth, circuit parameters of the piezoelectric stack are optimized so as to trace adaptively the peak-absorption trajectory. As a result, acoustic resistance–reactance path of the meta-composite has been reshaped so that more numbers of frequency points are distributed near the impedance matching point. Theoretical results have good agreements with numerical ones.

Our absorptive meta-composites are of deep subwavelength sizes and function as high acoustic absorption at low frequencies. One could achieve either tunable narrow-band or broadband sound absorption by tuning circuit parameters of the piezoelectric film and stack online, without changing the geometric structure of absorptive metamaterials. The proposed adaptive metamaterials are practically realizable, and expected to pave a new route towards the tunable and broadband sound absorption at extremely low frequencies.

Acknowledgments

This work is supported by the National Natural Science Foundation of China (Grant Nos. 11622215, 11572039, 11872111, and 11521062), and 111 project (B16003). The support from the Air Force Office of Scientific Research under Grant No. AF 9550-18-1-0342 with Program Manager Dr Byung-Lip (Les) Lee is also acknowledged.

ORCID iDs

Xiaoming Zhou https://orcid.org/0000-0002-3240-9789
Guoliang Huang https://orcid.org/0000-0003-0959-8427

References

[1] Yang M and Sheng P 2017 Sound absorption structures: from porous media to acoustic metamaterials *Annu. Rev. Mater. Res.* **47** 83–114
[2] Maa D Y 1998 Potential of microperforated panel absorber *J. Acoust. Soc. Am.* **104** 2861–6
[3] Maa D Y 2007 Practical single MPP absorber *Int. J. Acoust. Vib.* **12** 8
[4] Sui N, Yan X, Huang T-Y, Xu J, Yuan F-G and Jing Y 2015 A lightweight yet sound-proof honeycomb acoustic metamaterial *Appl. Phys. Lett.* **106** 171905
[5] Gao N, Wu J H, Yu L and Xin H 2016 Design of radial phononic crystal using annular soft material with low-frequency resonant elastic structures *Phys. Lett.* A **380** 3326–32
[6] Gao N, Hou H, Wu J H and Cheng B 2016 Low frequency band gaps below 10 Hz in radial flexible elastic metamaterial plate *J. Phys. D: Appl. Phys.* **49** 435501
[7] Yang M, Chen S, Fu C and Sheng P 2017 Optimal sound-absorbing structures *Mater. Horiz.* **4** 673–80
[8] Mei J, Ma G, Yang M, Yang Z, Wen W and Sheng P 2012 Dark acoustic metamaterials as super absorbers for low-frequency sound *Nat. Commun.* **3** 756
[9] Ma G, Yang M, Xiao S, Yang Z and Sheng P 2014 Acoustic metasurface with hybrid resonances *Nat. Mater.* **13** 873–8
[10] Cai X, Guo Q, Hu G and Yang J 2014 Ultrathin low-frequency sound absorbing panels based on coplanar spiral tubes or coplanar Helmholtz resonators *Appl. Phys. Lett.* **105** 121901
[11] Li Y and Assouar B M 2016 Acoustic metasurface-based perfect absorber with deep subwavelength thickness *Appl. Phys. Lett.* **108** 063502
[12] Chen C, Du Z, Hu G and Yang J 2017 A low-frequency sound absorbing material with subwavelength thickness *Appl. Phys. Lett.* **110** 221903
[13] Yang M, Meng C, Fu C, Li Y, Yang Z and Sheng P 2015 Subwavelength total acoustic absorption with degenerate resonators *Appl. Phys. Lett.* **107** 104104
[14] Li J, Wang W, Xie Y, Popa B-I and Cummer S A 2016 A sound absorbing metasurface with coupled resonators *Appl. Phys. Lett.* **109** 091908
[15] Fu C, Zhang X, Yang M, Xiao S and Yang Z 2017 Hybrid membrane resonators for multiple frequency asymmetric absorption and reflection in large waveguide *Appl. Phys. Lett.* **110** 021901
[16] Wei P, Croënne C, Tak Chu S and Li J 2014 Symmetrical and anti-symmetrical coherent perfect absorption for acoustic waves *Appl. Phys. Lett.* **104** 121902
[17] Meng C, Zhang X, Tang S T, Yang M and Yang Z 2017 Acoustic coherent perfect absorbers as sensitive null detectors *Sci. Rep.* **7** 43574
[18] Kuo S M and Morgan D R 1999 Active noise control: a tutorial review *Proc. IEEE* **87** 943–73
[19] Mokry P, Fukada E and Yamamoto K 2003 Sound absorbing system as an application of the active elasticity control technique *J. Appl. Phys.* **94** 7356–62
[20] Chang D, Liu B and Li X 2010 An electromechanical low frequency panel sound absorber *J. Acoust. Soc. Am.* **128** 639–45
[21] Duan X, Wang H, Li Z, Zhu L, Chen R, Kong D and Zhao Z 2015 Sound absorption of a flexible micro-perforated panel absorber based on PVDF piezoelectric film *App. Acous.* **88** 84–9
[22] Galland M A, Mazeaud B and Sellen N 2005 Hybrid passive/active absorbers for flow ducts *App. Acous.* **66** 691–708
[23] Sitel A and Galland M A 2011 Scattering-matrix formulation for both measurement and prediction of acoustical performances of hybrid cells and their active and passive elements *Acta Acust. U. Acust.* **97** 579–89
[24] Canevet G 1978 Active sound absorption in an air conditioning duct *J. Sound Vib.* **58** 333–45
[25] Dupont J-B and Galland M-A 2009 Active absorption to reduce the noise transmitted out of an enclosure *App. Acous.* **70** 142–52
[26] Lissek H, Boulandet R and Fleury R 2011 Electroacoustic absorbers: bridging the gap between shunt loudspeakers and active sound absorption *J. Acoust. Soc. Am.* **129** 2968–78
[27] Li X, Chen Y, Hu G and Huang G 2018 A self-adaptive metamaterial beam with digitally controlled resonators for subwavelength broadband flexural wave attenuation *Smart Mater. Struct.* **27** 045015
[28] Chen Y Y, Hu G K and Huang G L 2016 An adaptive metamaterial beam with hybrid shunting circuits for extremely broadband control of flexural waves *Smart Mater. Struct.* **25** 105036
[29] Liao Y, Chen Y, Huang G and Zhou X 2018 Broadband low-frequency sound isolation by lightweight adaptive metamaterials *J. Appl. Phys.* **123** 091705

[30] Skvor Z 1991 *Vibrating Systems and their Equivalent Circuits* (Amsterdam: Elsevier)

[31] Bongard F, Lissek H and Mosig J R 2010 Acoustic transmission line metamaterial with negative/zero/positive refractive index *Phys. Rev.* B **82** 094306

[32] Hagood N W and Vonflotow A 1991 Damping of structural vibrations with piezoelectric materials and passive electrical networks *J. Sound Vib.* **146** 243–68

[33] Kinsler L E, Frey A R, Coppens A B and Sanders J V 1999 *Fundamentals of Acoustics* (New York: Wiley)

[34] Zhang H, Wen J, Xiao Y, Wang G and Wen X 2015 Sound transmission loss of metamaterial thin plates with periodic subwavelength arrays of shunted piezoelectric patches *J. Sound Vib.* **343** 104–20

[35] Wang G, Wang J, Chen S and Wen J 2011 Vibration attenuations induced by periodic arrays of piezoelectric patches connected by enhanced resonant shunting circuits *Smart Mater. Struct.* **20** 125019

[36] Soedel W 2004 *Vibrations of Shells and Plates* (New York: Dekker)